Effect of electrospinning parameters on the mechanical and morphological characteristics of small diameter PCL tissue engineered blood vessel scaffolds having distinct micro and nano fibre populations – A DOE approach

R.A. O'Connor [a,b], P.A. Cahill [b], G.B. McGuinness [a,*]

[a] Centre for Medical Engineering Research, School of Mechanical and Manufacturing Engineering, Dublin City University, Dublin 9, Ireland
[b] Vascular Biology and Therapeutics Laboratory, School of Biotechnology, Dublin City University, Dublin 9, Ireland

A B S T R A C T

Electrospinning is a widely used technique in tissue engineered blood vessel (TEBV) scaffold research. Successful TEBV scaffolds must be produced in a way that balances tissue-like mechanical characteristics with morphologies that promote cellularity by supporting cell attachment whilst also permitting cell infiltration. Electrospun tubular poly (ε-caprolactone) (PCL) scaffolds combining interspersed nano and micro fibre morphologies have shown promise in this regard. A comprehensive design of experiments (DOE) approach examines the effect of production parameters on the mechanical and morphological properties of small diameter PCL vascular scaffolds created using a single-step electrospinning process and comprised of multi-modal fibre populations. Mechanical properties of the vessels are assessed using a modified uniaxial ringlet tensile test method while morphological properties, including mean fibre diameter, degree of fibre alignment and porosity, are also captured.

Regression analysis showed that a diverse range of mechanical properties could be achieved through the careful adjustment of processing conditions. Constructs with a broad range of ultimate tensile strengths (~4–10 MPa) and Young's moduli (~1.5–3 MPa) were prepared. The speed of the rotating collector system was found to be a dominant factor influencing both the mechanical and morphological attributes of the fabricated scaffolds. Several other main effects and interactions terms were found to influence the scaffold attributes, including degree of fibre orientation and mean fibre diameter.

The potential applicability of particular tubular scaffolds for vascular applications were then evaluated by comparison with literature obtained mechanical property values for human coronary arteries and the great saphenous vein. This study demonstrates an important step towards a readily available and tailorable set of multi-modal PCL scaffold designs for further biological and clinical investigation.

1. Introduction

Electrospinning has been widely examined as a route to achieving morphologically and biomechanically compatible scaffolds for tissue engineered blood vessel (TEBV) development. While electrospun nanofibre scaffolds have been shown to demonstrate increased cell adherence and proliferation properties compared to their micron fibre counterparts [1–3], they typically suffer from limited cell infiltration impacting long-term matrix deposition [4–7]. This lack of cell infiltration is typically attributed to the small size, complex distribution, and lack of pore connectivity within the nanofibre constructs [8]. Hence a

structure comprised of several distinct interspersed fibre diameter populations may offer increased void spaces for cell infiltration via a less dense microfibre superstructure, while simultaneously supporting cell attachment and proliferation through the presence of an intermixed nanofibre subpopulation.

Gentsch and colleagues first investigated electrospinning of bi-modal fibre distributions for enhanced cell infiltration properties using a polycaprolactone (PCL)/chloroform solution. The fibre structures produced contained highly elongated beads indicating the non-uniform stretching of micron fibres towards the nanoscale [9]. De Valence et al. later created PCL vascular grafts exhibiting multi-modal fibre populations

using chloroform/ethanol solutions. The addition of ethanol to the spinning solution induced increased splaying effects within the electrospinning jet, aiding the onset of uniform nanofibre formation [10]. The implanted scaffolds maintained patency and were free of aneurysm formation after 18 months implantation. At 6 weeks, the entire thickness of the graft was sparsely infiltrated by macrophages and fibroblasts. The cell population further increased up to 12 months, at which point a regression was observed. The extent of cell invasion at 18 months was comparable to that at 6 weeks, at about 25%, leaving areas of sparse cellularity in the centre of the graft wall.

Though clearly a promising avenue, the creation of architectures to promote and maintain full cellularity in electrospun TEBV's requires more study. Therefore, the objective of this study was to establish detailed protocols for the creation of small diameter (ø6 mm) tubular vessels with the desired multimodal fibre morphologies, and determine the effects of the production parameters on both the fibre architectures and the vessel wall mechanical properties.

To establish the effects of several electrospinning processing parameters on the mechanical and morphological attributes of multimodal fibre scaffolds, a factorial regression analysis is presented. Regression analysis provides a method to obtain a first order approximation for the dependence of output responses on corresponding input parameters, through the systematic and randomised variation of factor combinations referred to as 'treatments' [11]. Four process parameters commonly associated with electrospinning were selected as predictor variables (X) namely, solution flow rate (X_1), applied voltage (X_2), tip to collector distance (X_3) and the rotational speed of the collection surface (X_4). As the mechanical and morphological properties of electrospun scaffolds are known to be instrumental factors for defining overall scaffold function and for driving cell differentiation [12], they were identified as key descriptor variables (Y) of interest. Mechanical properties including the ultimate tensile strength (Y_1) and Young's modulus (Y_2) are crucial for determining the scaffolds ability to resist pulsatile loading forces while also preventing compliance mismatch issues between native tissue that may lead to eventual graft occlusion [13,14]. UTS and YM properties of the tubular scaffolds were assessed using a modified uniaxial tensile test designed for vascular prostheses [15].

Scaffold porosity (ε) is a morphological property known to dictate the efficient exchange of nutrients, gases, and waste products within the scaffold body. As porosity is crucial to cell migration and engraftment, it was selected for study (Y_3). Additional morphological properties known to influence electrospun scaffold performance are mean fibre diameter and degree of fibre alignment reported as Y_4 and Y_5, respectively. These parameters are known to influence the attachment, proliferation and differentiation of cells seeded on tissue engineered constructs [1,2,16]. Table 1 outlines the summarised predictor (X) and descriptor (Y) variables investigated as part of the regression study along with the

treatment levels assessed for each predictor variable. A final comparison is made between the mechanical properties of the multimodal PCL scaffolds produced to that of native tissue structures including human coronary arteries (HCA) and the Great Saphenous Vein (GSV) with the goal of establishing their suitability for future TEBV development.

2. Materials and methods

2.1. Materials

Poly (ε-caprolactone) with an average molecular weight (Mw) of 80,000 g/mol was purchased from Sigma Aldrich (USA). The following solvents & surfactants were employed: Chloroform (≥99%) with amylenes as a stabiliser (Sigma Aldrich), Ethanol (≥99.5, 200 proof) (Sigma Aldrich) and Methanol (≥99.8) (Fluka).

2.2. Solution preparation and characterisation

2.2.1. Solution preparation

Electrospinning solutions were prepared by dissolving a desired concentration of 16 wt% PCL in Chloroform/Ethanol. PCL was premixed in Chloroform for 2 h under constant stirring at room temperature (21 ± 1 °C) after which the surfactant ethanol was slowly added at a volume ratio of 7:3 as required. The final solution was mixed for a further 22 h to achieve homogeneity. Solutions were kept sealed until required and used within 4 days post preparation.

2.2.2. Viscosity & conductivity assessment

Solution viscosity was assessed using a Brookfield DV-II + Pro viscometer with a CPA-40Z cone attached. Calibration of the viscometer was performed using two Poly (dimethylsiloxane) (PDMS) standards of 100 cSt and 500 cSt at 25 °C (Sigma Aldrich). Electrospinning solutions were maintained at a temperature of 25 °C in the viscometer chamber during testing. Solution conductivity was assessed using a modified HD 8706 conductivity meter with a PTFE probe guard. Calibration was verified using three potassium chloride standard solutions (A-C, Fluka). Before measuring the reagents and solutions were heated and maintained at a temperature of 25 °C. Three batches of each reagent were prepared for viscosity and conductivity assessment to ensure the uniformity of the preparation protocol.

2.3. Electrospinning of small diameter tubular scaffolds

Small diameter tubular scaffolds were electrospun using a custom designed and fabricated rotating mandrel system as shown in Fig. 1 (A). In brief the system employed a rotating copper mandrel (ø6 mm) as the target collector. To enhance the uniformity of deposition the mandrel traversed with respect to the needle tip at a velocity of 0.6 m/s and amplitude of 14 cm. Three replicate vessels (n = 3) were produced for each parameter permutation of the regression analysis (Table 1). Following electrospinning the tubular scaffolds were released from their mandrel's by immersing in 100% methanol for 1 h [17]. The final constructs were dried at room temperature for 72 h prior to further testing (B). Several 10 mm long ringlet specimens were harvested from each vessel for mechanical and morphological analysis.

2.4. SEM characterisation of electrospun membranes

Morphological characterisation of electrospun samples was performed using an EVO LS15 Scanning Electron Microscope (Zeiss, Germany). 10 mm long ringlet specimens harvested from the tubular scaffolds were cut open along their longitudinal axis to form a flat membrane and a section taken for imaging. Samples were coated with a thin layer of gold (Scancoat, US), and viewed with an acceleration voltage of 10–15 kV. Image J image processing software was utilised to measure the diameter of thirty fibres (n = 30) for each sample produced.
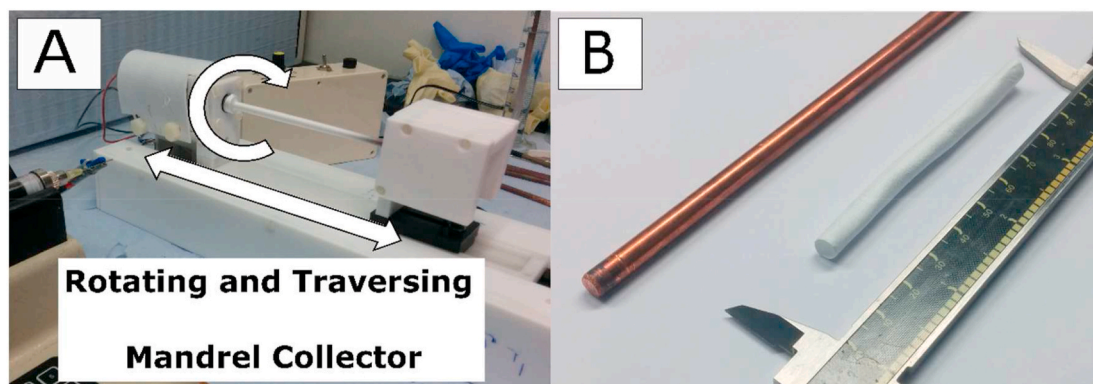
Table 1
Predictor variables under investigation as part of the multimodal regression analysis with corresponding treatment levels along with the descriptor variables selected for analysis.

	Label	Parameter	Unit	Treatment Level		
				−1	0	+1
Predictor	X_1	Flow rate (FR)	ml/hr	4	8	12
	X_2	Applied Voltage (AV)	kV	15	–	20
	X_3	Distance (D)	cm	15	17.5	20
	X_4	Collection Speed (CS)	RPM	1600	–	3200
Descriptor	Y_1	Ultimate Tensile Stress (UTS)	MPa			
	Y_2	Youngs's Modulus (YM)	MPa			
	Y_3	Porosity (ε)	%			
	Y_4	Mean Fibre Diameter	μm			
	Y_5	Degree of Fibre Alignment (Coherency)	–			

Fig. 1. Electrospinning of three-dimensional tubular scaffolds (A) Rotating mandrel rig indicating traversing motion and direction of mandrel rotation (B) PCL tubular scaffold removed from copper mandrel following methanol removal step.

The Image J plugin 'Orientation J' was used to measure the accompanying degree of fibre alignment with a coherency term generated for each image [18]. A coherency value of 1 indicates fibre structures possess a single dominant orientation, while a value of 0 represents an isotropic fibre network. A colour map is overlaid onto the output images to provide a visual representation of fibre orientation, with fibres displaying a similar colour indicating a common orientation.

2.5. Porosity

Porosity of the PCL scaffolds were assessed using the liquid intrusion technique. In this method the dry weight of 10 mm long ringlet specimens harvested from the scaffold were first measured. Samples were subsequently immersed in 100% ethanol for 24 h under agitation to ensure complete wetting. The samples were subsequently removed, and the surfaces blotted dry to remove excess fluids. The wet weight was then measured, and the porosity (ε) calculated using the following formulas:

$$V_{PCL} = \frac{m_{dry}}{\rho_{PCL}} \tag{1}$$

$$V_{EtOH} = \frac{m_{wet} - m_{dry}}{\rho_{EtOH}} \tag{2}$$

$$Porosity\ (\varepsilon) = \frac{V_{EtOH}}{V_{PCL} - V_{EtOH}} x\ 100\% \tag{3}$$

Where V_{PCL} is the volume of PCL within the sample and V_{EtOH} is the volume of ethanol entrapped in the scaffold pores. m_{dry} and m_{wet} refer to the dry and wet weights of the samples respectively while ρ_{EtOH} is the density of ethanol (0.789 g cm^{-3}) and ρ_{PCL} is the density of PCL (1.145 g cm^{-3}).

2.6. Uniaxial tensile testing of ringlet specimens

An adapted uniaxial test method as described within ISO 7198 for the testing of tubular vascular grafts was used to assess the mechanical characteristics of the produced scaffolds [19]. A Zwick Z005 tensile testing machine with a 500 N load cell and custom-built pin grip fixtures as shown in Fig. 2 was employed. The grips consisted of ⌀1.5 mm mounting pins with a centre to centre spacing of 2.5 mm at test commencement. Ringlet specimens were placed over the two mounting and subsequently separated by a unidirectional load until failure at a rate of 10 mm/min.

Prior to testing the ringlet specimens were hydrated in PBS for 24 h at 37 °C. The internal (D$_i$) and external diameters (D$_o$) of the ringlets were measured using a Mitutoyo light microscope with a toolmakers micrometer. Two orthogonal orientations were assessed to obtain an average specimen diameter used to calculate the wall thickness (t). The longitudinal length (L) of the ringlet samples were measured using a Vernier callipers. Subsequently the stress within the sample was calculated based on a cross sectional area of $2*t*L$ accounting for two wall segments resisting load [20].
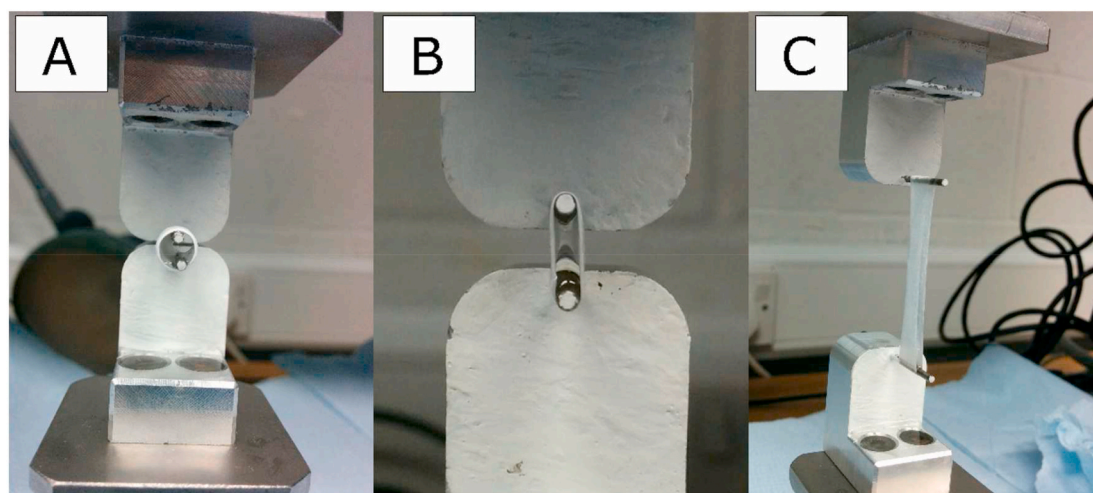

Fig. 2. Uniaxial ringlet tensile test method (A) Sample prior to loading (B) Sample showing vessel walls aligned to the direction of loading at which strain is normalised to 0% in post processing steps (C) Sample of image after testing.

The gauge length (L_o) of the sample was determined by calculating the distance between the centre of the loading pins when the vessel walls aligned parallel to the direction of loading without any overall perimeter change compared to the non-loaded state. This value was calculated based on the D_i and D_o values measured. Using this information, the captured strain profile was normalised to zero at the point when vessel wall alignment was deemed to have occurred. Failure to account for the reconfiguration of the sample during loaded results in an artificially large initial toe region that misrepresents the true stress-strain profile leading to unreliable Young's modulus and strain at break measurements.

2.7. Statistical analysis

Numerical data is presented as mean ± standard deviation (S.D). The design and analysis of the factorial regression study was conducted using the statistical software package Minitab 17.

3. Results & discussion

3.1. Electrospinning of small diameter tubular scaffolds

Solutions of 16 wt% PCL dissolved in Chloroform/Ethanol (7:3; v:v) with a viscosity range of 495.8 ± 4.3 mPa s and conductivity of 0.3 ± 0.0 μS/cm were prepared for the production of electrospun multi-modal fibre scaffolds. A factorial regression analysis comprising 36 treatments was studied to identify the key processing parameters that affect the mechanical and morphological attributes of the scaffolds namely; ultimate tensile strength (Y_1), Young's modulus (Y_2), porosity (Y_3), mean fibre diameter (Y_4) and degree of fibre alignment (Y_5).

Fig. 3 shows representative SEM images (with coherency colour-map overlay) outlining the multi-modal architecture of the collected scaffolds along with the corresponding stress-strain profiles obtained through ringlet tensile testing. Using these findings, the descriptor variables of interest were calculated and input into the regression design. To reduce the complexity of the final calculated model, a stepwise elimination approach was utilised to remove or 'drop' non-significant predictor terms from the final numerical model ($p > 0.05$). For each of the terms found to be significant a coefficient value was assigned that indicates its contribution to the output response with a larger value indicating greater significance. A positive coefficient indicates that the output response increases as the corresponding level of the input parameter is increased, while a negative coefficient indicates a reduction to the output response with increasing input value. Due to the substantial number of regression model outputs generated for each descriptor term, the stepwise elimination table and graphical outputs is presented in full for the single descriptor term, UTS (Y_1). The complete set of regression models for the remaining descriptor terms may be found in the accompanying supplementary data with the main findings discussed with regards to the predictor terms studied.

3.1.1. Effect of collection speed

Table 2 shows the tabulated results of the regression model analysis performed for UTS. Here the coefficient terms for both the full and reduced model are presented along with the p-value used to determine if a parameter should be kept or dropped from the final model. The ranking system indicates the importance of the final terms contribution to the model. Briefly, several parameters were found to have a significant effect in predicting the UTS properties of the electrospun vessels, with the dominant parameter being that of the rotational speed of the collection mandrel. Increasing the rotational speed was found to result in superior UTS properties, with vessels possessing an average of ~1.9 MPa at 1600 RPM and ~2.4 MPa at 3200 RPM (Fig. 4). This is attributed to an increased degree of fibre alignment within the scaffolds allowing
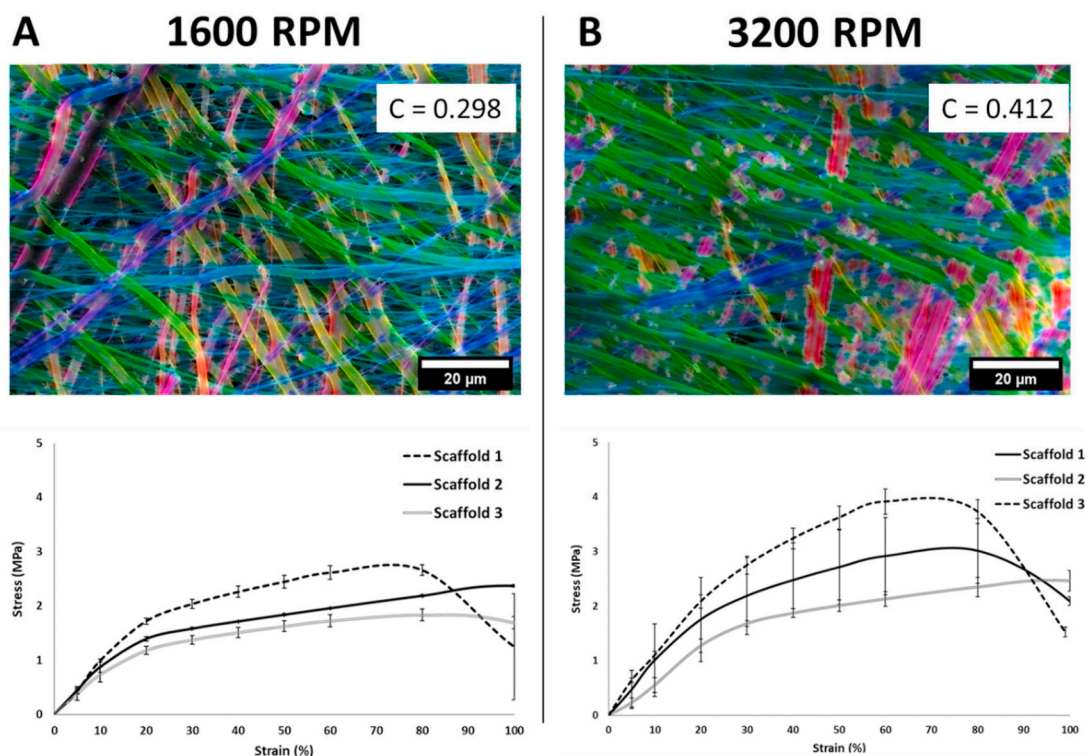

Fig. 3. SEM images of multi-modal electrospun samples created at a flow rate of 4 ml/h, applied voltage of 15 kV and collection distance of 17.5 cm with their fibre orientation colour map overlayed, along with the accompanying stress-strain response of the tubular specimens assessed using a modified uniaxial ringlet tensile test (A) Scaffolds specimens prepared at lower mandrel rotational speed of 1600 RPM with a degree of fibre alignment (coherency) of 0.298 (B) Scaffold specimens prepared at the increased mandrel rotational speed of 3200 RPM showing increased degree of fibre alignment (coherency) of 0.412. (For interpretation of the references to colour in this figure legend, the reader is referred to the Web version of this article.)

Table 2

Regression model analysis of output variable UTS (Y_1) obtained by stepwise elimination modelling (p > 0.05) where FR = solution flow rate, AV = applied voltage, D = distance from spinneret tip to collector surface & CS = rotational speed of collection mandrel.

|	Main Effect/Interaction	P	Coefficients Full Model	t-Value	Keep/Drop	Coefficients in Reduced Model	Ranking
1	Constant	0.000	2.1861	91.51	Keep	2.1861	(0)
2	X_1 (FR)	0.016	−0.0720	−2.46	Keep	−0.0720	6,7
3	X_2 (AV)	0.652	−0.0108	−0.45	Drop	−	
4	X_3 (D)	0.000	−0.1426	−4.87	Keep	−0.1426	2
5	X_4 (CS)	0.000	0.2190	9.17	Keep	0.2190	1
6	X_1*X_2	0.043	0.0600	2.05	Keep	0.0600	9
7	X_1*X_3	0.000	−0.1341	−3.74	Keep	−0.1341	4
8	X_1*X_4	0.034	−0.0630	−2.15	Keep	−0.0630	8
9	X_2*X_3	0.051	−0.0578	−1.97	Drop	−	
10	X_2*X_4	0.009	−0.0635	−2.66	Keep	−0.0635	5
11	X_3*X_4	0.339	−0.281	−0.96	Drop	−	
12	$X_1*X_2*X_3$	0.016	0.0882	2.46	Keep	0.0882	6,7
13	$X_1*X_2*X_4$	0.483	0.0206	0.70	Drop	−	
14	$X_1*X_3*X_4$	0.220	−0.0442	−1.23	Drop	−	
15	$X_2*X_3*X_4$	0.081	−0.0517	−1.77	Drop	−	
16	$X_1*X_2*X_3*X_4$	0.000	0.1578	4.40	Keep	0.1578	3
17	Block	0.859	N/A	–	Drop	−	
	S	**R-Sq**	**R-Sq (adj)**	**R-Sq (pred)**			
Full	0.248262	66.10%	60.57%	53.02%			
Reduced	0.253481	62.36%	58.90%	53.79%			
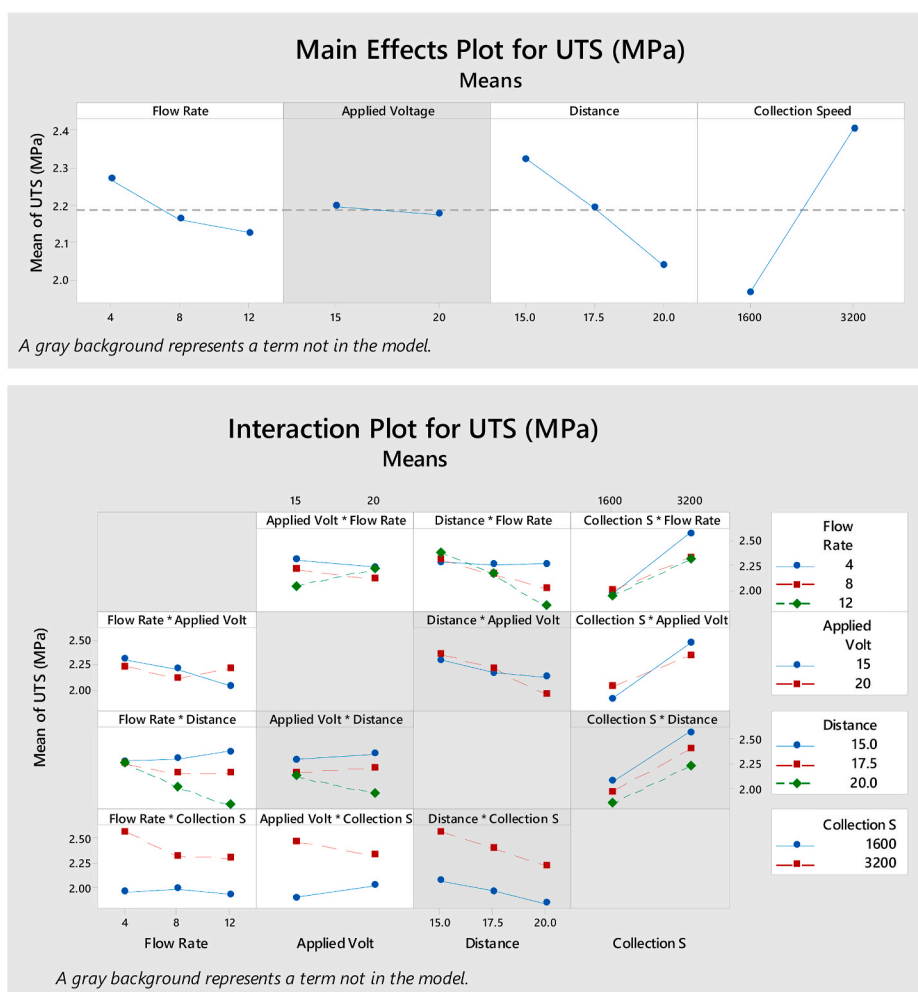
Fig. 4. Main effects and interaction plot for the regression variable UTS (Y_1) showing the effects of changing predictor levels to the response variable of interest. Greyed backgrounds represent a main effect term or interaction not included within the reduced model used to predict the output response.

for greater load distribution whilst also increasing their packing density, thereby reducing the cross-sectional area used to calculate the UTS [20]. These results are supported by the regression models produced for scaffold porosity (Supplementary Table S2 & Figure S2), mean fibre diameter (Table S3 and Figure S3) and degree of fibre alignment (Table S4 & Figure S4) where collection speed was found to be a

significant predictor term for all. The mean diameter of the collected fibres was observed to decrease (~1.17 μm–~1.03 μm) while the degree of fibre alignment increased (~0.205–0.255) as the collection speed increased from 1600 to 3200 RPM. This is anticipated to occur due to the tensile forces imparted upon the depositing fibres due to the rotational motion of the collector surface [21]. In turn collection speed was found to be the most significant parameter to affect porosity, with a small average decrease from ~84% to 83% as the speed was increased. An increase in fibre packing density may also explain the rise in Young's modulus observed from ~6.0 MPa to ~7.1 MPa with increasing collector speed.

3.1.2. Effect of tip-to-collector distance

Increasing the distance between the capillary tip and collector surface was also found to result in reduced UTS properties with average values of ~2.3 MPa at 15 cm and ~2.0 MPa at 20 cm observed. YM properties of scaffolds conversely increased with increasing collector distance, from ~5.7 at 15 cm to ~7.4 MPa at 20 cm. (Table S1 & Figure S1). This is suspected to occur due to the reduction of fused fibre junctions at the increased collector distances, due to enhanced solvent evaporation rates before deposition [22]. While increased fibre connectivity typically results in increased UTS properties it may also reduce the ability of fibres to re-orientate upon the application of an applied load [23]. This inability to align to the direction of loading may subsequently result in decreased Young's modulus characteristics at lower collector distances.

3.1.3. Effect of flow rate

As commonly observed in electrospinning applications [24], flow rate was observed to significantly alter the diameter of the fibres produced. Fibre diameters were found to increase from an average of ~1.02 μm–1.14 μm at 4 ml/h and 8 ml/h, respectively. No further increase in fibre diameter was observed between 8 and 12 ml/h. An unexpected finding was the reduction of UTS with increasing flow rate. This did not correlate with experimental observations wherein vessels produced at the increased flow rate possessed increased wall thicknesses and appeared to be more rigid compared to those produced at the lower flow rates aiding in post-processing manipulation. This is suspected to occur due to increased void volumes created with scaffold's wall due to the natural crossing of larger nonwoven fibres formed at the higher flow rates. Increased void volumes result in a reduced fibre density and thus larger cross-sectional area used to compute the ultimate tensile stress. In parallel with what was observed within the analysis of the UTS response, Young's modulus was similarly found to decrease with increasing flow rate. It is again suspected that this decrease occurred due to the decrease in fibre density within the scaffold walls resulting in disproportionate increase in cross sectional areas between vessels fabricated at lower flow rates compared to those at higher flow rates.

3.2. Effect of applied voltage

While applied voltage was not found to be a significant predictor for the overall mechanical properties of the scaffold it was found to be an important parameter to dictate morphological attributes. A reduction of both fibre diameter and fibre orientation were observed for increasing applied voltage. Increasing the applied voltage typically led to the initiation of smaller offspring jets from the Taylor's cone. These smaller jets aid and enhance the presence of nanofibre deposition within the scaffolds [25]. Increased applied voltage also increases the electrostatic field strength resulting in the rapid deposit to the mandrel and thus not undergoing re-orientation upon contact with the rotating surface [26].

3.2.1. General comments

An important aspect of the final regression models produced is the R-sq and R-sq (pred) values obtained. High R-sq and R-sq (pred) values indicate that the regression model accurately describes the results of the

experimental data whilst also possessing the ability to accurately predict future observations [27]. The final model for UTS yielded R-Sq and R-sq (pred) values of 62.36% and 53.79%, respectively. These values suggest that while significant main effects and interaction terms were identified from the model, that not all data was wholly explained by the descriptor terms studied. This is attributed to the complex nature of the electrospinning approach that is highly influenced by numerous solution, environmental and processing parameters. Variations in solution characteristic such as viscosity may alter the mechanics of electrospinning jet giving rise to variations in the fibre constructs produced and thus their final mechanical and morphological properties [28]. This is supported by the R-sq and R-sq (pred) terms found for morphological properties which typically ranged from 20 to 30%. This again indicates that the descriptor terms selected did not fully describe the obtained data. The inherent multi-modal nature of the produced scaffold makes it difficult to describe the scaffold construct using a single predictor term such as mean fibre diameter while scaffold porosity does not provide a complete assessment of the complex pore structure within the scaffold body. While the models did not fully explain the experimental data in its entirety, they provide an important insight into the key parameters to leverage in future finer studies.

3.3. Suitability of tubular vessel mechanical properties for arterial applications

The tubular scaffolds produced using 16 wt% PCL Chloroform/Ethanol (7:3; v:v) solutions demonstrated average UTS values ranging from ~1.5 to 3 MPa. Previous studies have shown the circumferential tensile strength of native human coronary arteries (HCAs) to be 1.44 ± 0.87 MPa [29], and the gold standard vessel for arterial bypass grafting, the great saphenous vein (GSV) to be 3.01 ± 1.91 MPa [30]. The UTS values of the electrospun scaffolds are comparable to these biological tissues (Fig. 5) and are anticipated to have suitable resistance to loading when implanted. In addition, the scaffolds demonstrated Young's modulus properties ranging from ~4 to 10 MPa depending on the electrospinning permutation employed. Previous studies have in turn demonstrated the Young's modulus of HCAs to be 1.55 ± 0.52 MPa, and GSVs to be 42.62 ± 27.76 MPa. Other works have shown that porcine coronary arteries, a common conduit used in experimental studies for its mechanical resemblance to human tissue, exhibits Young's modulus values of ~4 ± 2 MPa [31]. While the electrospun vessels do not directly match any of these individual characteristics, they do fall within the overall range of properties for the biological tissues associated with arterial bypass applications. The successful matching of Young's modulus properties can be used as a screening indicator to ultimately develop a vessel with matching overall biomechanical characteristics.

4. Conclusions

Electrospun PCL tubular scaffolds comprised of multi-modal fibre diameter populations for the specific purpose of enhanced cell infiltration were created through the systematic design, screening and regression analysis of a single step electrospinning process. PCL scaffolds with distinct nano and micro fibre populations were created with comparable ultimate tensile strengths (UTS) and Young's moduli (YM) to published values for relevant arteries and conduits currently used in arterial bypass applications. Regression models were found to be capable of describing the significant main effects and interactions influencing the biomechanical properties of UTS and YM based on the key input parameters of flow rate, applied voltage, collector distance and collection speed. However, regression analysis metrics indicate that not all data for UTS was fully explained by the process descriptors studied, and that variation in solution properties might affect fibre formation and morphological properties which are poorly predicted by the selected process parameters alone. These models and data, provide insight which can enlighten and refine future studies in this area, while the fabricated electrospun
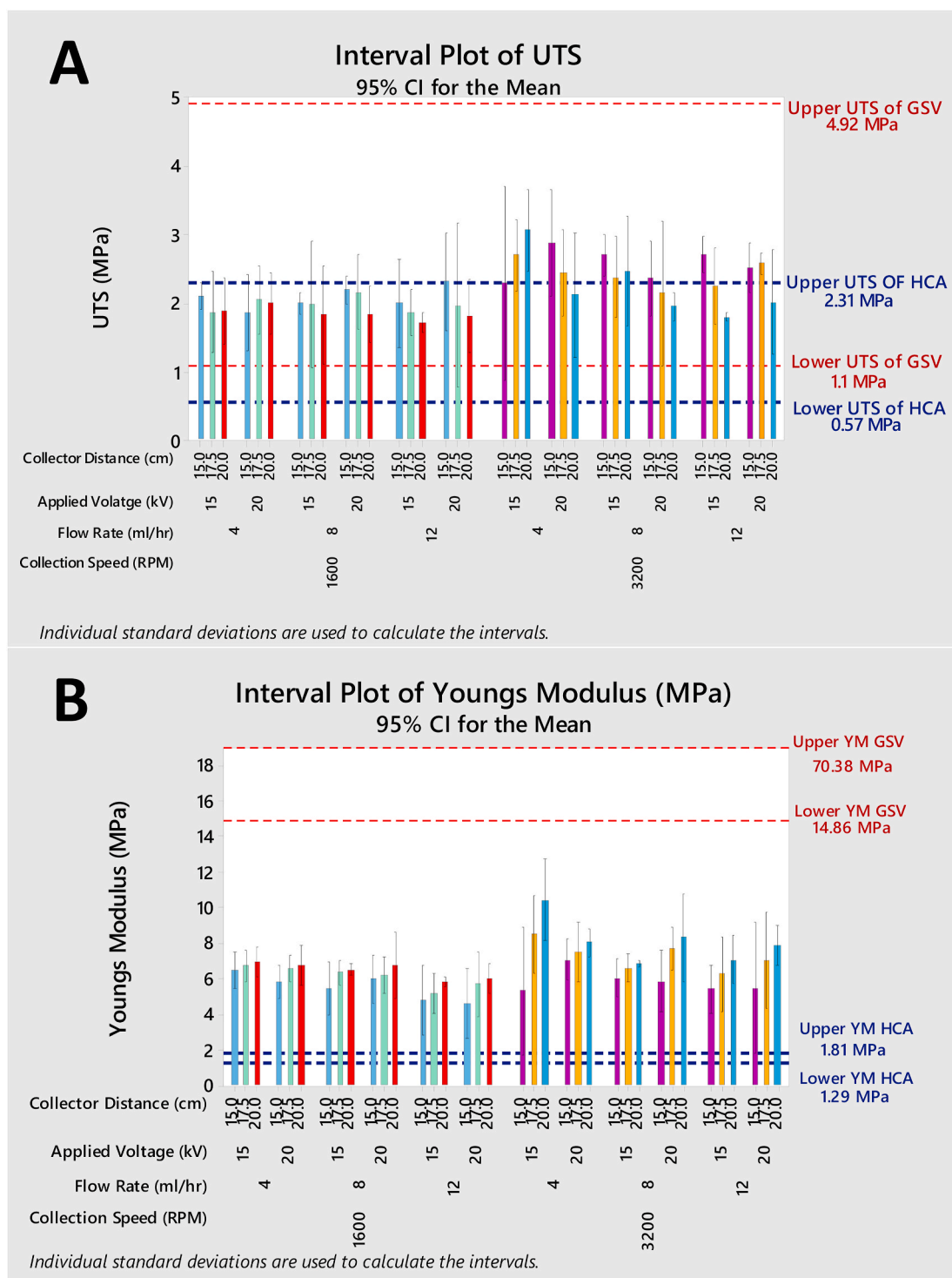
Fig. 5. UTS & Youngs' modulus responses for sample studies as part of the multimodal electrospinning experimental study, with lower and upper boundary ranges of common blood vessels indicated. Data for Human Coronary Arteries (HCAs) is adapted from Karimi et al. [29], and the Great Saphenous Vein (GSV) from Donovan et al. [30] (A) UTS Responses compared to biological vessels (B) Young's Modulus compared to biological vessels.

vessels developed will enable the systematic study of cell infiltration phenomena associated with these particular scaffold architectures.

CRediT authorship contribution statement

R.A. O'Connor: Conceptualization, Methodology, Validation, Formal analysis, Investigation, Data curation, Writing - original draft, Writing - review & editing, Visualization. **P.A. Cahill:** Conceptualization, Methodology, Resources, Writing - review & editing, Supervision. **G.B. McGuinness:** Conceptualization, Methodology, Resources, Writing - review & editing, Supervision, Project administration, Funding acquisition.

Declaration of competing interest

The authors declare that they have no known competing financial

interests or personal relationships that could have appeared to influence the work reported in this paper.

Acknowledgements

Appendix A. Supplementary data

Supplementary data to this article can be found online at https://doi.org/10.1016/j.polymertesting.2021.107119.

References

[1] S. Soliman, et al., Multiscale three-dimensional scaffolds for soft tissue engineering via multimodal electrospinning, Acta Biomater. 6 (4) (Apr. 2010) 1227–1237, https://doi.org/10.1016/j.actbio.2009.10.051.

[2] C.T. Laurencin, A.M.A. Ambrosio, M.D. Borden, J.A. Cooper, Tissue engineering: Orthopedic applications, Annu. Rev. Biomed. Eng. 1 (1) (Aug. 1999) 19–46, https://doi.org/10.1146/annurev.bioeng.1.1.19.

[3] A.I. Teixeira, G.A. Abrams, P.J. Bertics, C.J. Murphy, P.F. Nealey, Epithelial contact guidance on well-defined micro- and nanostructured substrates, J. Cell Sci. 116 (Pt 10) (May 2003) 1881–1892, https://doi.org/10.1242/jcs.00383.

[4] S. Zhong, Y. Zhang, C.T. Lim, Fabrication of large pores in electrospun nanofibrous scaffolds for cellular infiltration: a review, Tissue Eng. B Rev. 18 (2) (Apr. 2012) 77–87, https://doi.org/10.1089/ten.TEB.2011.0390.

[5] A. Martins, R.L. Reis, N.M. Neves, Electrospinning: processing technique for tissue engineering scaffolding, Int. Mater. Rev. 53 (5) (Sep. 2008) 257–274, https://doi.org/10.1179/174328008X353547.

[6] A. Martins, J. V Araújo, R.L. Reis, N.M. Neves, Electrospun nanostructured scaffolds for tissue engineering applications, Nanomedicine 2 (6) (Dec. 2007) 929–942, https://doi.org/10.2217/17435889.2.6.929.

[7] R.A. O'Connor, G.B. McGuinness, Electrospun nanofibre bundles and yarns for tissue engineering applications: a review, Proc. Inst. Mech. Eng. Part H J. Eng. Med. 230 (11) (2016) 987–998, https://doi.org/10.1177/0954411916656664.

[8] A. Hasan, et al., Electrospun scaffolds for tissue engineering of vascular grafts, Acta Biomater. 10 (1) (Jan. 2014) 11–25, https://doi.org/10.1016/j.actbio.2013.08.022.

[9] R. Gentsch, B. Boysen, A. Lankenau, H.G. Börner, Single-step electrospinning of bimodal fiber meshes for ease of cellular infiltration, Macromol. Rapid Commun. 31 (1) (2010) 59–64, https://doi.org/10.1002/marc.200900431.

[10] S. de Valence, et al., Long term performance of polycaprolactone vascular grafts in a rat abdominal aorta replacement model, Biomaterials 33 (1) (Jan. 2012) 38–47, https://doi.org/10.1016/j.biomaterials.2011.09.024.

[11] R. Seyedmahmoud, et al., A primer of statistical methods for correlating parameters and properties of electrospun poly(L-lactide) scaffolds for tissue engineering-Part 1: design of experiments, J. Biomed. Mater. Res. 103 (1) (Jan. 2015) 91–102, https://doi.org/10.1002/jbm.a.35153.

[12] J. Nam, J. Johnson, J.J. Lannutti, S. Agarwal, Modulation of embryonic mesenchymal progenitor cell differentiation via control over pure mechanical modulus in electrospun nanofibers, Acta Biomater. 7 (4) (2011) 1516–1524, https://doi.org/10.1016/j.actbio.2010.11.022.

[13] S. Sarkar, H.J. Salacinski, G. Hamilton, M. Seifalian, The mechanical properties of infrainguinal vascular bypass grafts: their role in influencing patency, Eur. J. Vasc. Endovasc. Surg. 31 (6) (2006) 627–636, https://doi.org/10.1016/j.ejvs.2006.01.006.

[14] P.D. Ballyk, C. Walsh, J. Butany, M. Ojha, Compliance mismatch may promote graft-artery intimal hyperplasia by altering suture-line stresses, J. Biomech. 31 (3) (1997) 229–237, https://doi.org/10.1016/S0197-3975(97)00111-5.

[15] S.H. Kim, C.H. Mun, Y. Jung, S.-H. Kim, D.-I. Kim, S.H. Kim, Mechanical properties of compliant double layered poly(L-lactide-co-ε-caprolactone) vascular graft, Macromol. Res. 21 (8) (2013) 886–891, https://doi.org/10.1007/s13233-013-1095-5.

[16] Z. Tan, H. Wang, X. Gao, T. Liu, Y. Tan, Composite vascular grafts with high cell infiltration by co-electrospinning, Mater. Sci. Eng. C 67 (Oct. 2016) 369–377, https://doi.org/10.1016/j.msec.2016.05.067.

[17] K.H. Lee, H.Y. Kim, M.S. Khil, Y.M. Ra, D.R. Lee, Characterization of nanostructured poly(ε-caprolactone) nonwoven mats via electrospinning, Polymer 44 (4) (Feb. 2003) 1287–1294, https://doi.org/10.1016/S0032-3861(02)00820-0.

[18] R. Rezakhaniha, et al., Experimental investigation of collagen waviness and orientation in the arterial adventitia using confocal laser scanning microscopy, Biomech. Model. Mechanobiol. 11 (3–4) (Mar. 2012) 461–473, https://doi.org/10.1007/s10237-011-0325-z.

[19] A. N. Standard, ISO 7198: Cardiovascular implants - tubular vascular prostheses 1–56 (2001).

[20] C. Del Gaudio, L. Fioravanzo, M. Folin, F. Marchi, E. Ercolani, A. Bianco, Electrospun tubular scaffolds: on the effectiveness of blending poly(ε-caprolactone) with poly(3-hydroxybutyrate- co -3-hydroxyvalerate), J. Biomed. Mater. Res. B Appl. Biomater. 100B (7) (Oct. 2012) 1883–1898, https://doi.org/10.1002/jbm.b.32756.

[21] M.J. McClure, S. a Sell, C.E. Ayres, D.G. Simpson, G.L. Bowlin, "Electrospinning-aligned and random polydioxanone–polycaprolactone–silk fibroin-blended scaffolds: geometry for a vascular matrix, Biomed. Mater. 4 (5) (Oct. 2009), 055010, https://doi.org/10.1088/1748-6041/4/5/055010.

[22] S.S. Zargarian, V. Haddadi-Asl, "A nanofibrous composite scaffold of PCL/Hydroxyapatite-chitosan/PVA prepared by electrospinning," Iran, Polym. J. 19 (6) (2010) 457–468.

[23] S. Shang, F. Yang, X. Cheng, X. Frank Walboomers, J.A. Jansen, The effect of electrospun fibre alignment on the behaviour of rat periodontal ligament cells, Eur. Cell. Mater. 19 (2010) 180–192, https://doi.org/10.22203/eCM.v019a18.

[24] S.H. Tan, R. Inai, M. Kotaki, S. Ramakrishna, Systematic parameter study for ultra-fine fiber fabrication via electrospinning process, Polymer 46 (16) (Jul. 2005) 6128–6134, https://doi.org/10.1016/j.polymer.2005.05.068.

[25] J.M. Deitzel, J. Kleinmeyer, D. Harris, N.C. Beck Tan, The effect of processing variables on the morphology of electrospun nanofibers and textiles, Polymer 42 (1) (2001) 261–272, https://doi.org/10.1016/S0032-3861(00)00250-0.

[26] C. Ribeiro, V. Sencadas, C.M. Costa, J.L. Gómez Ribelles, S. Lanceros-Méndez, Tailoring the morphology and crystallinity of poly(L-lactide acid) electrospun membranes, Sci. Technol. Adv. Mater. 12 (1) (2011), https://doi.org/10.1088/1468-6996/12/1/015001.

[27] R. Dorati, et al., The effect of process parameters on alignment of tubular electrospun nanofibers for tissue regeneration purposes, J. Drug Deliv. Sci. Technol. 58 (May) (2020), 101781, https://doi.org/10.1016/j.jddst.2020.101781.

[28] Z. Li, C. Wang, Effects of working parameters on electrospinning, One-Dimensional nanostructures (2013) 15–29, https://doi.org/10.1007/978-3-642-36427-3.

[29] A. Karimi, M. Navidbakhsh, A. Shojaei, S. Faghihi, Measurement of the uniaxial mechanical properties of healthy and atherosclerotic human coronary arteries, Mater. Sci. Eng. C 33 (5) (Jul. 2013) 2550–2554, https://doi.org/10.1016/j.msec.2013.02.016.

[30] D.L. Donovan, S.P. Schmidt, S.P. Townshend, G.O. Njus, W. V Sharp, Material and structural characterization of human saphenous vein, J. Vasc. Surg. Off. Publ. Soc. Vasc. Surg. [and] Int. Soc. Cardiovasc. Surgery, North Am. Chapter 12 (5) (1990) 531–537.

[31] E.M. Campbell, Investigation of Small-Diameter Decellularised Artery as a Potential Scaffold for Vascular Tissue Engineering, " Dublin City University, 2013.